STRUCTURAL BIOLOGY COMMUNICATIONS

ISSN 2053-230X

Crystal structure of *Arabidopsis thaliana* casein kinase 2 α1

Manon Demulder,[a,b,c] Lieven De Veylder[c,d] and Remy Loris[a,b]*

[a]Structural Biology Brussels, Vrije Universiteit Brussel, Pleinlaan 2, B-1050 Brussels, Belgium, [b]Center for Structural Biology, VIB, Pleinlaan 2, B-1050 Brussels, Belgium, [c]Department of Plant Biotechnology and Bioinformatics, Ghent University, Technologiepark 71, B-9052 Ghent, Belgium, and [d]Center for Plant Systems Biology, VIB, Technologiepark 71, B-9052 Ghent, Belgium. *Correspondence e-mail: remy.loris@vub.be

Received 27 January 2020
Accepted 1 April 2020

Edited by M. W. Bowler, European Molecular Biology Laboratory, France

Keywords: casein kinase; CK2; structural flexibility; ATP binding; *Arabidopsis thaliana*.

PDB references: casein kinase 2 α1, 6xx6; 6xx8; 6xx9; complex with AMppNHp, 6xx7

Supporting information: this article has supporting information at journals.iucr.org/f

Casein kinase 2 (CK2) is a ubiquitous pleiotropic enzyme that is highly conserved across eukaryotic kingdoms. CK2 is singular amongst kinases as it is highly rigid and constitutively active. *Arabidopsis thaliana* is widely used as a model system in molecular plant research; the biological functions of *A. thaliana* CK2 are well studied *in vivo* and many of its substrates have been identified. Here, crystal structures of the α subunit of *A. thaliana* CK2 in three crystal forms and of its complex with the nonhydrolyzable ATP analog AMppNHp are presented. While the C-lobe of the enzyme is highly rigid, structural plasticity is observed for the N-lobe. Small but significant displacements within the active cleft are necessary in order to avoid steric clashes with the AMppNHp molecule. Binding of AMppNHp is influenced by a rigid-body motion of the N-lobe that was not previously recognized in maize CK2.

1. Introduction

Casein kinase 2 (CK2) is a serine/threonine kinase that is present in all eukaryotes. It is a distant member of the CMGC group of kinases, which also includes the CDK and MAPK kinases. Individual families within this group tend to be highly conserved, and this is also the case for CK2. The CK2 holoenzyme is composed of two CK2 α catalytic subunits and two CK2 β regulatory units and is present as a dynamic tetrameric complex in the cell (Niefind *et al.*, 2001). While the β subunit is present as a single-copy gene within the human genome, two different genes encode the CK2 α′ and α″ subunits (Lozeman *et al.*, 1990). In contrast, multiple gene copies are present in plant genomes (Velez-Bermudez *et al.*, 2011). For instance, *Arabidopsis thaliana* encodes four α genes and four β genes. Three of the corresponding CK2 α proteins are located in the nucleus, while one is found in chloroplasts. All CK2 β proteins are found in the nucleus and to a smaller extent in the cytosol (Salinas *et al.*, 2006). The combinatorial options to compose a full CK2 complex from the different CK2 α and β subunits influences the activity and substrate specificity (Janeczko *et al.*, 2011). The β subunits within the holo complex fulfill multiple roles such as fine-tuning substrate specificity in plants (Dennis & Browning, 2009), guiding the formation of the CK2 complex and enhancing catalytic activity. Yet, *in vitro*, the α subunit on its own is sufficient for enzymatic activity. Using either ATP or GTP, CK2 will phosphorylate a S/T-D/E-*X*-D/E consensus sequence, where the P + 1 and P + 3 acidic residues are crucial (for a review, see Meggio & Pinna, 2003).

CK2 activity is highly pleiotropic (Meggio & Pinna, 2003; Bian *et al.*, 2013). In mammals, about 300 substrates have been

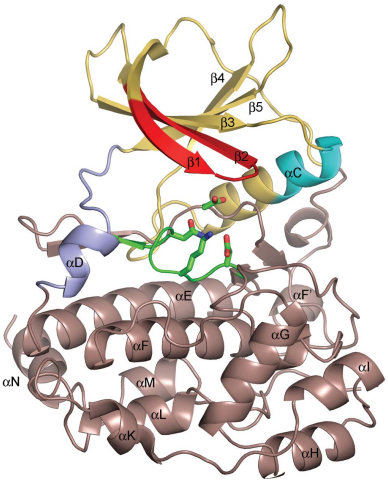

Table 1
Macromolecule-production information.

Construct	CK2 α-His
Source organism	*A. thaliana*
DNA source	*A. thaliana*
Forward primer†	ATACATATGTCGAAAGCTCGTGTGTACACCG
Reverse primer‡	AGTGGATCCTCATTGACTTCTCATTCTGCTGG
Cloning vector	pET-23d(+)
Expression vector	pET-23d(+)
Expression host	*E. coli* BL21 (DE3)
Complete amino-acid sequence of the expressed proteins	See Fig. 1

† At-CK2A1 5′ NdeI (Dennis & Browning, 2009). ‡ At-CK2A1 3′ BamHI (Dennis & Browning, 2009).

identified. In contrast, as yet only 30 substrates have been confirmed for plant CK2 (Vilela *et al.*, 2015). Nonetheless, plant CK2 is active in diverse pathways related to the cell cycle, DNA-damage response and repair (Moreno-Romero *et al.*, 2012), biotic and abiotic stress response, hormonal response, phosphate homeostasis (Chen *et al.*, 2015), light-sensitivity and the circadian clock (Marta *et al.*, 2013). Moreover, in addition to the role of the holoenzyme, both the α and β subunits seem to have independent roles in the cell (Bibby & Litchfield, 2005).

Currently, a large body of structures are available for the human and maize CK2s (Niefind *et al.*, 1998; Battistutta, Sarno, De Moliner, Marin *et al.*, 2000; Battistutta, Sarno, De Moliner, Papinutto *et al.*, 2000; Niefind *et al.*, 2001). These mostly consist of structures of the isolated α subunit in its free state, in complex with ATP or an ATP analog, or in complex with inhibitory small-molecule compounds (for reviews, see Niefind *et al.*, 2009; Kinoshita *et al.*, 2013). CK2 α structures have also been determined for several yeast species (PDB entries 6ise, 6o6q and 4fi1) and for the parasite *Plasmodium falciparum* (PDB entry 5xvu) (Liu *et al.*, 2014; Ruiz-Carrillo *et al.*, 2018; Ong *et al.*, 2019). CK2 has been recognized as a druggable target and many structures of human and maize CK2 in complex with inhibitory compounds are available in the PDB. In both human and maize CK2, the ATP-binding site is a hotspot for small-molecule CK2 inhibitors, which function via the steric exclusion of ATP (see, for example, Tsuyuguchi *et al.*, 2020; Niefind *et al.*, 2017; Golub *et al.*, 2013; Ferguson *et al.*, 2011; Niefind & Issinger, 2010). In human CK2, a second binding site for inhibitors was suggested at the binding interface with the β subunit. Initially, this site was identified in the structure of the complex with 5,6-dichloro-1-β-D-ribofuranosylbenzimidazole (DRB) (Raaf *et al.*, 2008). It has been argued that this site behaves as an allosteric inhibition site because in this structure, as well as in an isomorphous structure in which glycerol is found at the same site, the ATP-binding region adopts an apparently inactive conformation (Raaf *et al.*, 2008). DRB, however, also binds to the canonical ATP-binding cleft and therefore there is no direct proof that binding of DBR via this second site on its own inhibits CK2 activity. Other compounds that bind to this region have since been identified and these compete with the binding of CK2 β and modulate the catalytic activity of human CK2 α (Raaf *et al.*, 2013; Kufareva *et al.*, 2019).

A. thaliana is widely used as a model system in molecular plant research; the biological functions of *A. thaliana* CK2 have been well studied *in vivo* and many of its substrates have been identified (for a review, see Mulekar & Huq, 2014). Yet, the structure of *A. thaliana* CK2, and more broadly those of CK2s from eudicots in general, has not been described. Within the context of a larger project aiming at the identification of CK2 substrates in *Arabidopsis*, we present here the structure of the α1 subunit of *A. thaliana* casein kinase 2 in the presence and absence of AMppNHp.

2. Materials and methods

2.1. Cloning, protein expression and purification

The expression vector pET-23d(+) encoding *A. thaliana* CK2 α1 (TAIR accession No. At5g67380; Dennis & Browning, 2009) was kindly provided by Professor K. Browning, University of Texas at Austin, USA. Details of the construct are summarized in Table 1. Our construct lacks the first 75 amino acids as predicted from the At5g67380 sequence and corresponds to the coding sequence for the CK2 domain as found in all other CK2 sequences. The pET-23d(+) vector was transformed into *Escherichia coli* BL21(DE3) cells. The cell cultures were grown in LB medium and induced with 0.5 m*M* isopropyl β-D-1-thiogalactopyranoside when an OD_{600} of 0.6 was reached. After 3 h of induction at 30°C, the cells were harvested and resuspended in 50 m*M* Tris pH 7.5, 500 m*M* NaCl, 10% glycerol supplemented with cOmplete Protease Inhibitor Cocktail (Sigma). The cells were sonicated and the resulting cell lysate was pelleted for 1 h at 19 000 rev min^{-1} (4°C). The cell lysate was filtered and loaded onto a pre-equilibrated 1 ml Ni–NTA column. The tagged protein was separated from most contaminants using a stepwise imidazole gradient and was finally eluted by applying 500 m*M* imidazole. Fractions were pooled and concentrated before application onto a HiLoad Superdex 16/60 column pre-equilibrated with 25 m*M* Tris pH 7.5, 150 m*M* NaCl, 1 m*M* TCEP. The protein eluted from the column as a single peak and the purity of the protein was confirmed by 12% SDS–PAGE.

2.2. Crystallization and data collection

The protein was concentrated to 7 mg ml^{-1} in 25 m*M* Tris pH 7.5, 150 m*M* NaCl, 1 m*M* TCEP. Hanging-drop crystallization screens were set up manually with drops consisting of 1 µl protein solution and 1 µl precipitant solution equilibrated against 300 µl precipitant solution at 20°C. Plates were set up using screens from Hampton Research and the PACT *premier* and MIDAS Gold screens. For AMppNHp co-crystallization, the protein stock was supplemented with 10 m*M* AMppNHp and 1.5 m*M* $MgCl_2$.

Crystals were obtained in two conditions from the PACT *premier* screen. The best diffracting crystals were obtained using 0.2 *M* sodium sulfate, 0.1 *M* bis-Tris propane pH 6.5, 20% PEG 3350. Crystals were fished out and immersed in cryoprotectant solution (precipitant solution with the PEG

Table 2
Data collection and processing.

Values in parentheses are for the outer shell.

Crystal	CK2 α1 form I	CK2 α1 form II	CK2 α1 form III	CK2 α1 + AMppNHp
Crystallization				
Protein solution	25 m*M* Tris pH 7.5, 150 m*M* NaCl, 1 m*M* TCEP	25 m*M* Tris pH 7.5, 150 m*M* NaCl, 1 m*M* TCEP	25 m*M* Tris pH 7.5, 150 m*M* NaCl, 1 m*M* TCEP	25 m*M* Tris pH 7.5, 150 m*M* NaCl, 1 m*M* TCEP, 10 m*M* AMppNHp, 1.5 m*M* $MgCl_2$
Precipitant solution	0.2 *M* sodium sulfate, 0.1 *M* bis-Tris propane pH 6.5, 20% PEG 3350	0.2 *M* sodium sulfate, 0.1 *M* bis-Tris propane pH 6.5, 20% PEG 3350	0.2 *M* sodium sulfate, 0.1 *M* bis-Tris propane pH 6.5, 20% PEG 3350	0.2 *M* sodium sulfate, 0.1 *M* bis-Tris propane pH 6.5, 20% PEG 3350
Diffraction source	PROXIMA 2A	PROXIMA 1	PROXIMA 2A	PROXIMA 2A
Wavelength (Å)	0.9801	0.9785	0.9801	0.9801
Temperature (K)	100	100	100	100
Detector	EIGER X 9M	EIGER X 9M	EIGER X 9M	EIGER X 9M
Crystal-to-detector distance (mm)	254.78	189.59	296.87	280.843
Rotation range per image (°)	0.025	0.100	0.100	0.025
Total rotation range (°)	150	360	250	240
Space group	$P4_12_12$	$P2_1$	$P2_1$	$P4_12_12$
a, *b*, *c* (Å)	61.98, 61.98, 227.73	47.85, 81.17, 83.46	53.41, 62.22, 62.08	60.56, 60.56, 228.60
α, β, γ (°)	90.0, 90.0, 90.0	90.0, 105.17, 90.0	90.0, 106.75, 90.0	90.0, 90.0, 90.0
Mosaicity (°)	0.105	0.135	0.226	0.209
Resolution range (Å)	50.0–1.85 (1.96–1.85)	46.2–1.78 (1.89–1.78)	50.0–1.85 (1.95–1.84)	50.0–2.4 (2.54–2.40)
Total No. of reflections	323438 (18380)	403291 (56925)	145819 (15155)	292784 (39655)
No. of unique reflections	38664 (5815)	57878 (8433)	33248 (4699)	17625 (2711)
Completeness (%)	98.7 (94.2)	96.9 (89.2)	97.4 (85.5)	99.6 (97.8)
Multiplicity	8.4 (3.2)	7.1 (6.8)	4.4 (3.3)	16.6 (14.6)
$\langle I/\sigma(I)\rangle$	13.4 (1.0)	8.0 (0.5)	12.0 (1.0)	10.2 (1.3)
R_{merge}	0.092 (0.735)	0.125 (3.660)	0.063 (1.081)	0.237 (1.789)
R_{meas}	0.097 (0.878)	13.5 (3.954)	0.072 (1.279)	0.245 (1.853)
$CC_{1/2}$ (%)	99.8 (70.4)	99.8 (17.1)	99.9 (62.0)	99.7 (60.6)
Overall *B* factor from Wilson plot ($Å^2$)	34.3	45.2	42.5	52.6

3350 concentration increased to 30%) prior to flash-cooling in liquid nitrogen.

X-ray data were collected at 100 K on the PROXIMA 1 and PROXIMA 2A beamlines at the SOLEIL synchrotron source, Saint-Aubin, France. The data were indexed, scaled and merged with *XDS* (Kabsch, 2010) using the *xdsme* interface (Legrand, 2017). Data-collection and processing statistics are given in Table 2.

2.3. Structure determination and analysis

The structure of crystal form III was determined by molecular replacement using *Phaser* (McCoy *et al.*, 2007) with the coordinates of maize CK2 α1 (PDB entry 3pzh; E. Papinutto, A. Ranchio, G. Lolli, L. A. Pinna & R. Battistutta, unpublished work) stripped of water molecules as a search model. A clear solution was obtained with an LLG of 3656, and this solution was further refined using *phenix.refine* (Liebschner *et al.*, 2019) and rebuilt using *Coot* (Emsley *et al.*, 2010). A maximum-likelihood target was used throughout, and stereochemistry and ADP weights relative to the X-ray term were optimized. After the initial rigid-body refinement, a simulated-annealing step was introduced followed by alternating steps of manual rebuilding and refinement of individual *B* factors and coordinates and a single TLS group per chain. Water molecules were added when clear $F_o - F_o$ and $2F_o - F_o$ density was present at suitable distances (2.6–3.5 A) from potential hydrogen-bond donors or acceptors.

This model was then used to determine the structures of the other crystal forms as well as that of the complex with AMppNHp, again by molecular replacement, and the structures were rebuilt and refined using the same protocol as described for crystal form I. Secondary structure was assigned using the *DSSP* algorithm (Kabsch & Sander, 1983). Refinement statistics are summarized in Table 3.

3. Results and discussion

3.1. Structure of *A. thaliana* casein kinase 2

The α1 subunit of *A. thaliana* casein kinase 2 (TAIR accession No. At5g67380; referred to in the following as AtCK2) was heterologously expressed in *E. coli* BL21 cells. It is noteworthy that we used a construct that differed from the TAIR construct in that it was 75 amino acids shorter at the N-terminus. These 75 putative N-terminal residues were omitted because they encode a highly hydrophobic segment in the first 40 amino acids followed by a predicted disordered segment. As no other CK2 protein contains such an N-terminal extension and searches for orthologous sequences revealed no match to any other protein, this suggests a possible misannotation in the TAIR database. AtCK2 without this N-terminal extension has been studied as such as the active *A. thaliana* CK2 (Dennis & Browning, 2009).

AtCK2 was purified to homogeneity using Ni–NTA affinity chromatography, making use of its C-terminal His tag, followed by size-exclusion chromatography on a Superdex HiLoad 75 16/60 column. Crystallization screens led to the identification of two series of conditions that resulted in diffraction-quality crystals. The first series of conditions

involved PEG 3350 as a precipitant with Bis-Tris propane pH 6.5–7.5. These conditions led to three distinct crystal forms (Table 1), each of which diffracted to 1.8–1.85 Å resolution and contained a total of four independent AtCK2 monomers. Crystals were also observed in conditions containing 2.0 *M* ammonium sulfate, but were inferior in diffraction quality and were not pursued further.

All three structures were refined to R_{free} factors between 0.1945 and 0.2358 and displayed good stereochemistry. The overall structure consists of a single domain that can be split into two lobes (Fig. 1). The N-terminal lobe (N-lobe) encompasses residues Asp20–Ser113 and consists of a long, extended loop (residues 20–33), a five-stranded antiparallel β-sheet (residues 34–105) and a single four-turn α-helix (residues 70–84). The C-terminal lobe (C-lobe) is α-helical and contains various important motifs. The first is the glycine-rich hairpin (usually incorrectly referred to as a glycine-rich loop and also known as the ATP-binding loop), which is characterized by a G*X*G*X*φG sequence, where φ is usually a tyrosine or a phenylalanine residue (Huse & Kuriyan, 2002). In CK2 the last glycine is not conserved. This motif is common to all CMGC kinases (Pinna, 1997). The second motif is

Table 3
Refinement.

Values in parentheses are for the outer shell.

Crystal	CK2 α1 form I	CK2 α1 form II	CK2 α1 form III	CK2 α1 + AMppNHp
Resolution range	50.0–1.85 (1.91–1.85)	46.2–1.78 (1.85–1.78)	50.0–1.84 (1.86–1.84)	50.0–2.40 (2.57–2.40)
R_{work}	0.1725 (0.3558)	0.1991 (0.5385)	0.1991 (0.4758)	0.1949 (0.3405)
R_{free}	0.1945 (0.3702)	0.2358 (0.6039)	0.2268 (0.5781)	0.2467 (0.3705)
Total No. of protein chains	1	2	1	1
Total No. of protein atoms	2792	5244	2703	2655
Total No. of nonprotein atoms	376	267	180	105
R.m.s.d., bond lengths (Å)	0.0055	0.0050	0.0050	0.0025
R.m.s.d., bond angles (°)	0.67	0.79	0.83	0.53
Ramachandran most favored (%)	96.94	96.0	95.2	95.41
Ramachandran outliers (%)	0.0	0.6	0.9	0.6
Rotamer ouliers (%)	2.0	0.4	0.7	2.9
Clashscore	5.67	2.93	3.68	3.41
MolProbity score	1.71	1.35	1.49	1.81
Average *B* factor (Å^2)	33.8	51.4	52.8	59.7
PDB code	6xx6	6xx8	6xx9	6xx7

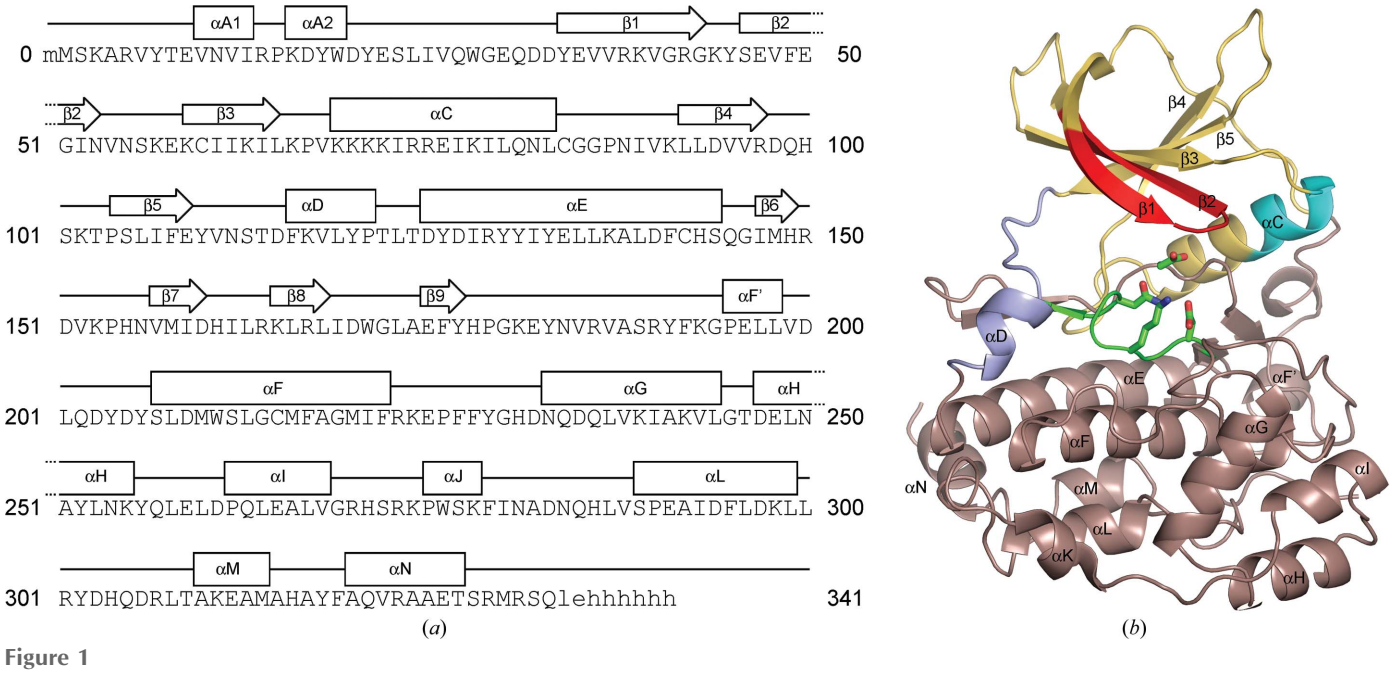

Figure 1
Overall structure of *A. thaliana* CK2 α1. (*a*) Amino-acid sequence of AtCK2 with the *DSSP*-derived secondary structure added. Residues in lower case letters correspond to cloning artifacts: an additional N-terminal methionine and a C-terminal His tag. Nomenclature of the secondary-structure elements is according to Niefind *et al.* (1998) and Marta *et al.* (2013) for the CMGC family of kinases, except that a short helix αF′ is added that is not present in this standard nomenclature. (*b*) Cartoon representation of AtCK2. Residues belonging to the N-lobe are colored orange/yellow and residues belonging to the C-lobe are colored brown. The Gly-rich/ATP-binding hairpin is indicated in red, the basic cluster in cyan, the hinge region in purple and the catalytic loop in green. Arg150, Asp151 and Asn156 in the catalytic loop as well as Asp170 in the loop between strands β8 and β9 are shown in green ball-and-stick representation.

formed by a stretch of basic residues (Lys–Arg75) located at the N-terminus of helix αC and is commonly referred to as the 'basic cluster'. This sequence is unique to CK2 kinases and has been suggested to be important for substrate recognition (Pinna, 1997; Sajnaga *et al.*, 2013).

The C-lobe encompasses residues Met1–Trp19 and Thr114–Arg329 and is mainly α-helical: nine α-helices of at least two turns are connected by a number of loops. This lobe contains the so-called catalytic loop that hosts Arg150, Asp151 and Asn156. The first residue, Arg150, is specific to the so-called 'RD kinases', of which CK2 is a member (Johnson *et al.*, 1996; Pinna & Meggio, 1997). The latter two residues are conserved in all kinases and are assumed to play a catalytic role (Huse & Kuriyan, 2002). It was established in cAMP-dependent protein kinase A (PKA) that the corresponding Asn aligns through hydrogen-bonding to the Asp residue for hydrophilic attack towards the hydroxyl group of the substrate. Outside the catalytic loop, the equivalent of Asp170 in AtCK2 was also found to be crucial to catalysis in PKA, probably by coordinating divalent cations during substrate binding.

The C-terminal residues Met330–Glu335, as well as the subsequent histidine tag, are disordered. The N-terminal methionine is also disordered in crystal form II, but clear density is observed for this methionine as well as for an additional preceding methionine (Met0) that results from a cloning artifact in crystal form III.

3.2. Structural variability and dynamics

Despite their similar resolutions, the three crystal forms are not equivalent in terms of the quality of the electron density and the corresponding atomic model. While in form I the backbone and most of the side chains are fully defined from Met1 to Arg329, form III has poor electron density for large parts of the N-lobe and a number of side chains in the C-lobe. Residues Arg14–Asp20 in chain *A* of crystal form II also lack interpretable electron density.

Superposition of the four crystallographically independent molecules resulting from the three crystal forms shows that the C-lobe is well defined in all structures and is highly rigid, with pairwise backbone r.m.s.d.s ranging between 0.186 and 0.364 Å. The N-lobe shows greater structural variability, with pairwise r.m.s.d.s ranging from 0.442 to 0.929 Å. This results from two distinct backbone conformations that are observed for the loop segment Ile64–Lys70 and small relative movements of the hairpin Val36–Ile52 and the the hairpin loop Arg97–Thr103 (Fig. 2*a*). However, we do not see any pronounced conformational differences in the hinge region (Tyr110–Leu123) including the αD helix.

We do see small rigid-body movements of the N-lobe relative to the C-lobe, with the two most extreme states being form I (more closed) and chain *A* of form II (more open) (Fig. 2*a*). Relative movement between the N- and C-lobes also occurs in other kinases. In the specific case of protein kinase A, it was found that autophosphorylation of the activation loop mediates a 18° relative movement of the N-lobe compared with the C-lobe (Steichen *et al.*, 2012). Different crystallization conditions probably allow the capture of distinct conformations that exist in solution.

Also notable is the previously mentioned poor electron density for the N-lobe of crystal form III. Here, electron density for residues His100–Lys102 is missing and density for Gly41–Ser46 is very weak. These two regions correspond to the β4–β5 hairpin loop and the glycine-rich hairpin, respectively. The β4–β5 hairpin loop forms the contact interface for oligomerization with CK2 β and displays a high conformational variability in human CK2 structures (Niefind *et al.*, 2009). The flexibility of the glycine-rich hairpin, which contacts the phosphates of AMppNHp, on the other hand, is relevant to CK2 catalytic activity (Huse & Kuriyan, 2002). Moreover, the electron density of the N-lobe in crystal form III is rather smeared out in the direction of the *a* axis, indicating an anisotropic movement that is absent in the much better-defined C-lobe. This dynamic nature of the N-lobe is also reflected in the distribution of *B* values, which are systematically higher for the N-lobe than for the C-lobe in all molecules, including in the well defined structure of crystal form I (Figs. 2*c*–2*e*).

3.3. ATP-binding site

AtCK2 was also crystallized in the presence of the non-hydrolyzable ATP analog AMppNHp at 10 m*M*. Clear electron density is visible for AMppNHp and a single Mg^{2+} ion located in a groove between the two lobes of AtCK2 (Fig. 3*a*). In addition to the AMppNHp molecule, the structure contains three chloride ions, a sulfate ion, a short stretch of PEG 3350 and 61 water molecules. The latter are all in common with the water molecules identified in the isomorphous crystal form I of the apo protein, despite the fact that the solvent structure of the latter was not used for as a guide to identify solvent atoms in the AMppNHp complex.

AMppNHp is well anchored in the active-site cleft formed by the catalytic loop, the glycine-rich hairpin loop and the hinge region before the αD helix (Fig. 3*b*). The adenine group of AMppNHp is sandwiched between the side chains of Val111, Met158 and Ile169 from the C-lobe on one side and of Val48 and Ile61 from the N-lobe on the other side, and makes hydrogen bonds to the backbone carbonyl of Glu109 and the backbone NH group of Val111. The triphosphate group hydrogen-bonds to two water molecules that are also conserved in the free structures as well as to the backbone O atom of Arg42 and the side chain of Ser46 in the glycine hairpin loop. The Mg^{2+} ion is coordinated by the side chains of His155, Asn156 and Asp170. The latter two residues are strictly conserved in all kinases, which shows that the proper orientation of divalent ions to compensate for the negative charge of the triphosphate is crucial to kinase activity (Pinna & Meggio, 1997). This arrangement is essentially identical to that previously found for AMppNHp binding to maize CK2 α (Niefind *et al.*, 1999), with the exception of a different rotamer conformation for His160 (His155 in AtCK2).

Since the crystal of the AMppNHp complex is isomorphous to crystal form I of the apo structure, a direct comparison of

the effect of AMppNHp binding to AtCK2 is possible without interference from packing effects. Overall, the glycine-rich hairpin and αD hinge adopt the 'open' conformation that is found in most deposited CK2 structures, compared with the more rarely sampled 'closed' conformation as found in DRB-bound human CK2 (PDB entry 3h30; Raaf *et al.*, 2008). When comparing our apo and AMppNHp-bound structures, two structural effects can be observed. The first one is minor and is located within the catalytic loop: a change in the rotamer conformation of His155 and the freezing of Met158 into a single conformation; the second minor conformation observed in crystal forms I and III is incompatible with AMppNHp binding. The second effect of AMppNHp binding on the structure of AtCK2 is a rigid-body rotation of 3.7° of the N-lobe (Figs. 3*c*–3*e*). This small but significant displacement is necessary in order to avoid steric clashes with the AMppNHp molecule. This movement is in agreement with the relative movements of the N-lobe seen in the three crystal forms of the free structure, with crystal forms II and III adopting somewhat intermediate conformations.

3.4. Trimethyl acetate

Crystal form I contains, besides protein and water, electron density that was interpreted as two chloride ions, a sulfate ion and a short worm-like stretch of density that was interpreted

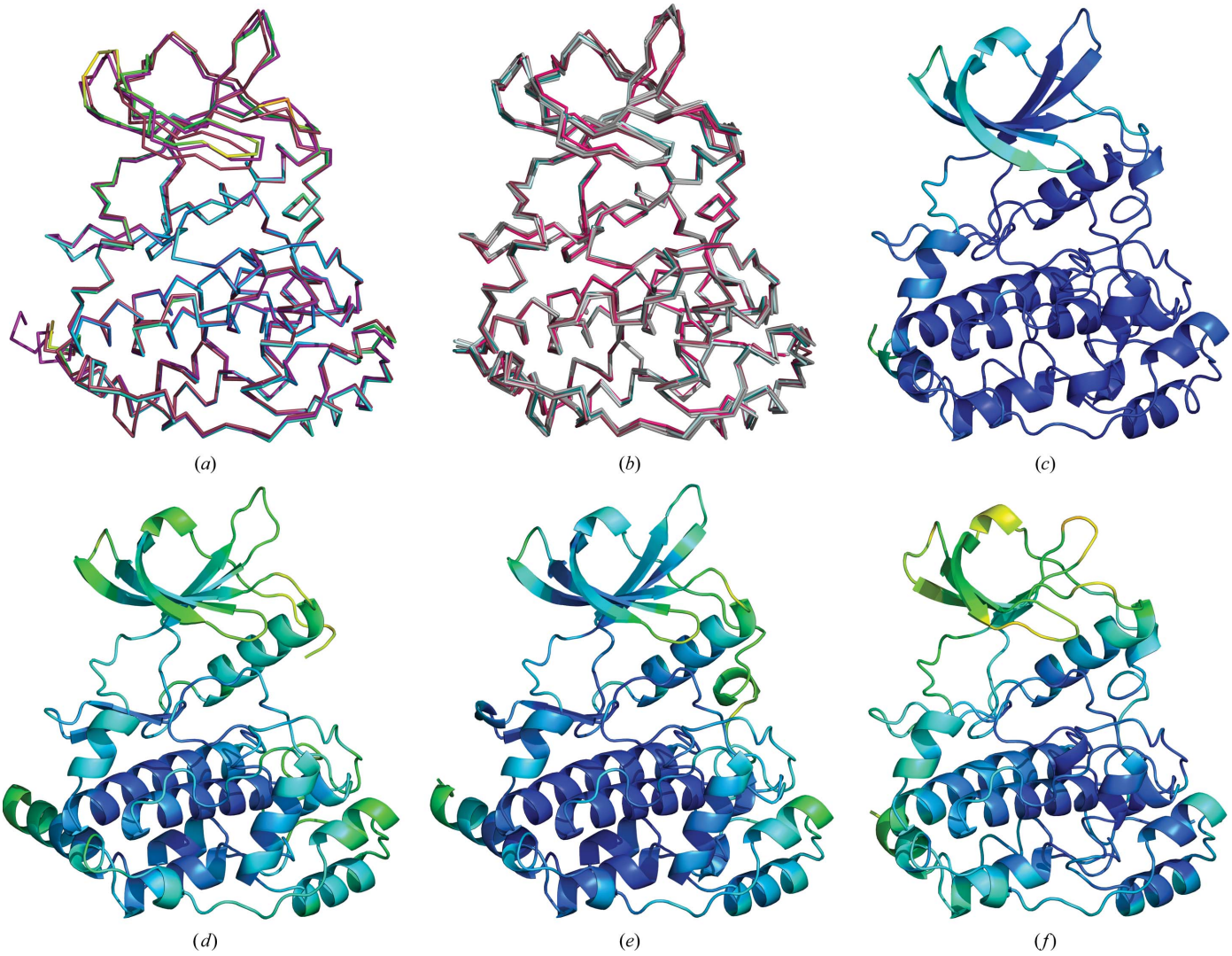

Figure 2
Structural flexibility. (*a*) Superposition of the C^{α} traces of the four independent molecules present in the asymmetric units of the three crystal forms of AtCK2 in its free state (form I in dark red, form II chain *A* in purple, form II chain *B* in gray and form III in orange). Near-perfect superposition is obtained for the C-lobe, while some structural variability is visible in the N-lobe. (*b*) Corresponding superposition for ZmCK2. The apo structure (PDB entry 1jam; Battistuta *et al.*, 2001) is in dark red, the ATP complex is in dark green (PDB entry 1daw; Niefind *et al.*, 1999), the GTP complex is in light green (PDB entry 1day; Niefind *et al.*, 1999), the complex with the β subunit is in purple (PDB entry 1ds5; Battistutta, Sarno, De Moliner, Marin *et al.*, 2000) and complexes with two ATP-competitive inhibitors are in gray (PDB entries 1zog, 3kxn and 4anm; Battistuta *et al.*, 2005; Samo *et al.*, 2011; Koltun *et al.*, 2012). (*c*–*f*) Cartoon representations of the four independent molecules present in the asymmetric units of the three crystal forms of AtCK2 in its free state (form I, form II chain *A*, form II chain *B* and form III, respectively) colored according to *B* factors. Dark blue indicates a low and red indicates a high *B* factor. While the absolute values vary, with form I having significantly lower *B* factors than the other crystal forms, the pattern of higher *B* factors in the N-lobe than in the C-lobe is universal.

as PEG 3350 based on the chemical contents of the crystallization mixture. It is also observed in the AMppNHp complex. There is, however, additional electron density that we interpreted as trimethyl acetate (pivalic acid; Fig. 4). The origin of this small molecule is not known, but the shape of the electron density is highly suggestive. The carboxylate group hydrogen-bonds to the main-chain NH group of Asp170 and the side chain of Lys63. The trimethyl group fills a hydrophobic crevice and makes hydrophobic van der Waals contacts with the side chains of Val48, Val90, Met158, Ile169, Phe108 and Ile61 and the aliphatic part of Lys63. These residues belong to both the N-lobe, including the glycine-rich hairpin, and the C-lobe, including the catalytic loop. The location of this trimethyl acetate molecule is such that its binding is sterically incompatible with the binding of AMppNHp, explaining its absence in the AMppNHp complex (Fig. 4).

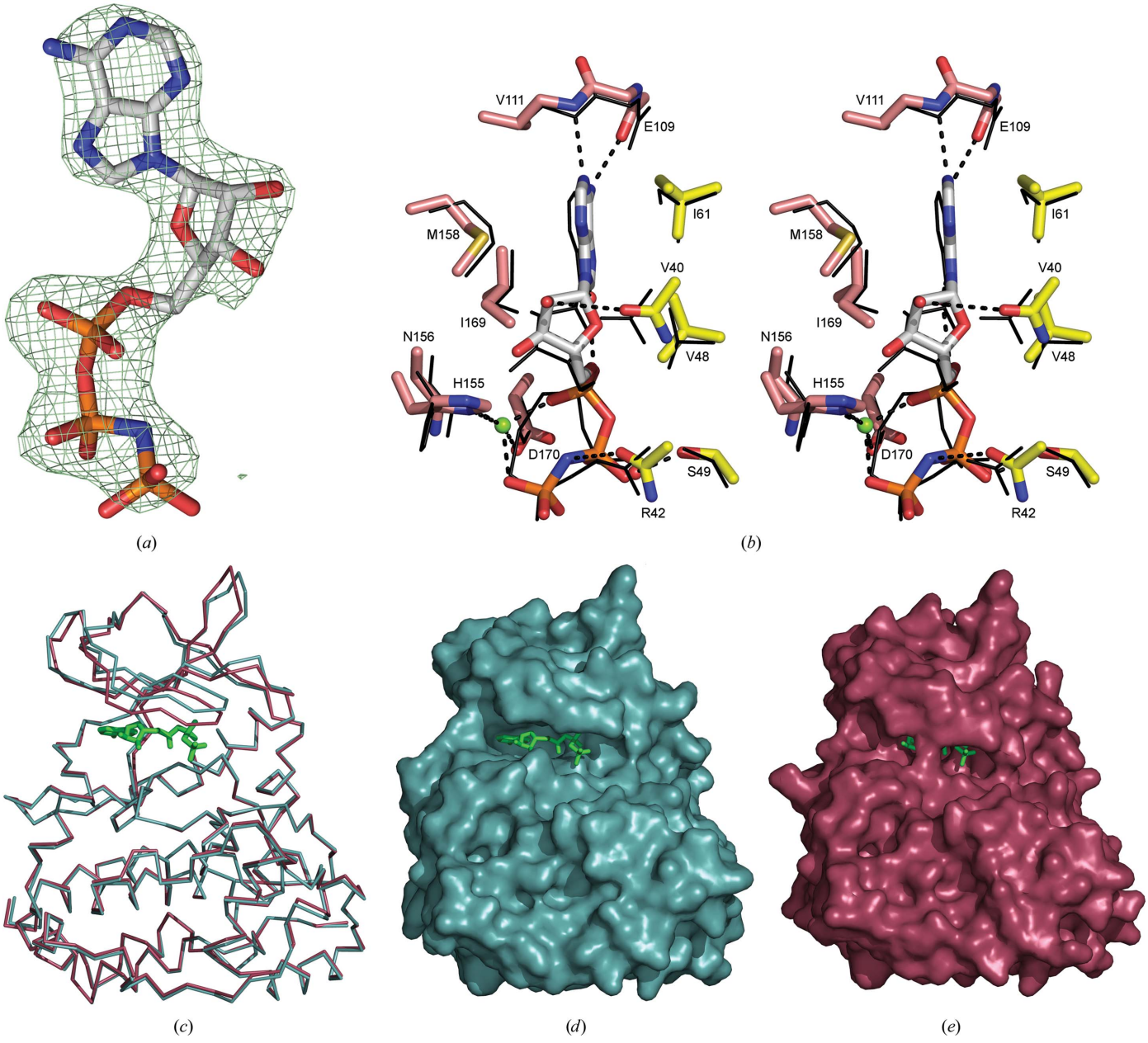

Figure 3
AMppNHp binding. (*a*) OMIT electron density of AMppNHp shown at 4σ. (*b*) Stereoview of the interactions of AMppNHp with the protein. All residues are labeled and colored according to atom type. Residues belonging to the N-lobe have their C atoms in yellow; residues from the C-lobe have their C atoms in brown. Water molecules are shown as red spheres and the Mg^{2+} ion as a green sphere. Hydrogen bonds and the coordination of the Mg^{2+} ion are indicated by dashed lines. The corresponding AMppNHp-binding site of maize CK2 is superimposed and shown as black lines. (*c*) Superposition of the C^{α} traces of form I and the AMppNHp complex, showing the small relative rotation of the N-lobe. The position of the AMppNHp molecule is indicated by a green stick model. (*d*) Surface representation of the AMppNHp complex showing how AMppNHp is located in the groove between the N-lobe and the C-lobe. (*e*) Equivalent surface representation of form I showing that the ATP-binding groove is narrowed and that in this conformation binding of AMppNHp would result in steric clashes.

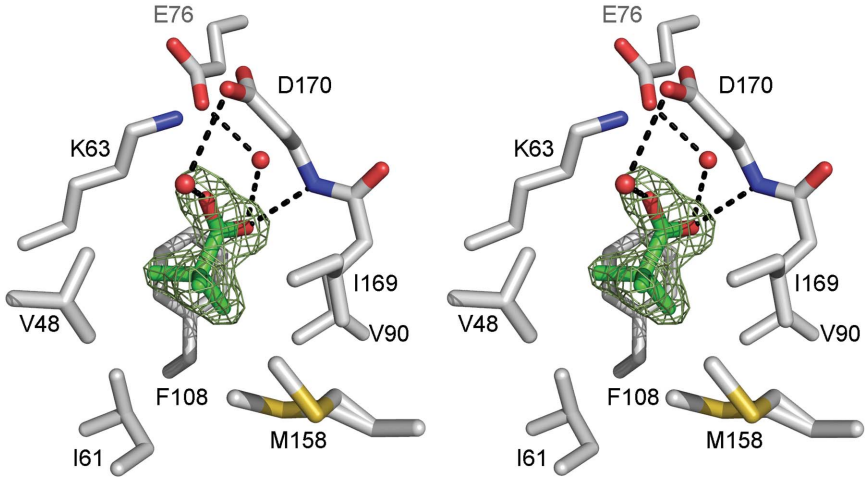

Figure 4
Binding of trimethyl acetate. Trimethyl acetate is shown with its C atoms in green, while the protein C atoms are colored gray. Water molecules are shown as red spheres. Contacting residues are labeled and the OMIT electron density for trimethyl acetate is shown at a level of 4σ. Several of the residues implicated in the binding of AMppNHp also contribute to the binding of trimethyl acetate.

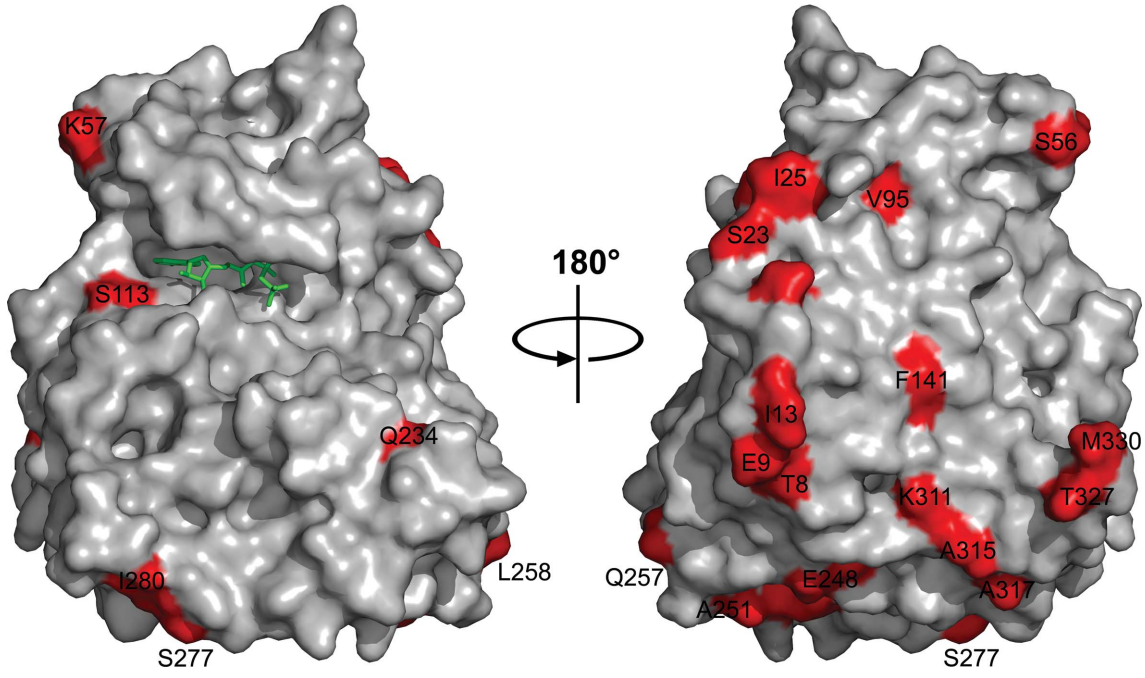

Figure 5
Arabidopsis versus maize CK2. Two views are shown 180° apart of a surface representation of the AMppNHp complex of AtCK2, with the amino acids that differ between the *Arabidopsis* and the maize enzymes indicated in red and labeled. The AMppNHp molecule is shown as a green stick model.

3.5. *Arabidopsis* versus maize CK2

Maize CK2 α (ZmCK2 α) displays 91% sequence identity to AtCK2. The 26 (out of 332) amino acids that are substituted between the proteins are scattered over the surface of the hemisphere opposite to the active site (Fig. 5). Only a single substitution (Ser113Asn) is located close to the AMppNHp-binding site, marginally touching the adenine group. Similarly, no amino-acid substitutions are observed between AtCK2 and ZmCK2 near the binding site of the β-subunit.

Neither the plasticity of the N-lobe nor its rigid-body motion relative to the C-lobe are observed in the various crystal structures of ZmC K2α in its free state, its AMppNHp-bound state or its complexes with various inhibitory compounds (Fig. 2*b*). All ZmCK2α structures show the open state. Possibly, this is a consequence of most structures being highly isomorphous to the ATP complex, making it possible that the open conformation is stabilized by lattice contacts.

4. Conclusion

Careful examination of human CK2 α crystal structures has led to the insight that although modest in comparison with other eukaryotic PK kinases, key conformational changes within human CK2 α allow regulatory control (Hochschref *et*

al., 2015). These involve open and closed conformations of the hinge region and of the glycine-rich ATP-binding hairpin loop. This conformational flexibility has not been observed in maize CK2 α, suggesting that this level of regulation might be absent in plant CK2s (Niefind *et al.*, 2009). In our structures of *Arabidopsis* CK2 α, we only observe the hinge region in its open conformation and also observe a single productive conformation for the ATP-binding hairpin loop. Whether the alternative inactive and partially inactive conformations described for human CK2 α can also occur in *Arabidopsis* cannot be ruled out based on this small ensemble of only four crystallographic independent molecules. The larger set of maize structures (with 91% sequence identity to *Arabidopsis*) does not add significantly to this given that they are mostly isomorphous to each other and the observed conformation(s) may be influenced by similar crystal-packing interactions. We do observe, however, a mechanism of regulation whereby the N-lobe can move as a rigid body relative to the C-lobe, thereby opening and closing the ATP-binding cleft. This movement is brought about by the flexible hinge in front of the αD helix. Likewise, the N-lobe of human CK2 has been described as relatively flexible, while this has not been observed in ZmCK2 structures (Niefind & Issinger, 2010). Based on molecular-dynamics simulations, such a regulatory mechanism has also been proposed for *Yarrowia lipolytica* CK2 α (Chaillot *et al.*, 2000), but no experimental evidence is yet available. In conclusion, it appears that, like human CK2, AtCK2 is relatively dynamic and can sample different conformational states. How these are populated within the cell at equilibrium remains to be uncovered.

Acknowledgements

We thank Professor K. Browning (University of Texas at Austin, USA) for providing the expression vector for *A. thaliana* CK2 α1.

Funding information

This work was supported by FWO grant G023616N to L. De Veylder, by FWO grant G011420N to L. De Veylder and R. Loris, and by VUB-OZR grant SPR13 to R. Loris. M. Demulder received a personal FWO SB PhD grant (1S18116N).

References

Battistutta, R., De Moliner, E., Sarno, S., Zanotti, G. & Pinna, L. A. (2001). *Protein Sci.* **10**, 2200–2206.
Battistutta, R., Mazzorana, M., Sarno, S., Kazimierczuk, Z., Zanotti, G. & Pinna, L. A. (2005). *Chem. Biol.* **12**, 1211–1219.
Battistutta, R., Sarno, S., De Moliner, E., Marin, O., Issinger, O.-G., Zanotti, G. & Pinna, L. A. (2000). *Eur. J. Biochem.* **267**, 5184–5190.
Battistutta, R., Sarno, S., De Moliner, E., Papinutto, E., Zanotti, G. & Pinna, L. A. (2000). *J. Biol. Chem.* **275**, 29618–29622.
Bian, Y., Ye, M., Wang, C., Cheng, K., Song, C., Dong, M., Pan, Y., Qin, H. & Zou, H. (2013). *Sci. Rep.* **3**, 3460.
Bibby, A. C. & Litchfield, D. W. (2005). *Int. J. Biol. Sci.* **1**, 67–79.
Chaillot, D., Declerck, N., Niefind, K., Schomburg, D., Chardot, T. & Meunier, J. C. (2000). *Protein Eng. Des. Sel.* **13**, 291–298.
Chen, J., Wang, Y., Wang, F., Yang, J., Gao, M., Li, C., Liu, Y., Liu, Y., Yamaji, N., Ma, J. F., Paz-Ares, J., Nussaume, L., Zhang, S., Yi, K., Wu, Z. & Wu, P. (2015). *Plant Cell*, **27**, 711–723.
Dennis, M. D. & Browning, K. S. (2009). *J. Biol. Chem.* **284**, 20602–20614.
Emsley, P., Lohkamp, B., Scott, W. G. & Cowtan, K. (2010). *Acta Cryst.* D**66**, 486–501.
Ferguson, A. D., Sheth, P. R., Basso, A. D., Paliwal, S., Gray, K., Fischmann, T. O. & Le, H. V. (2011). *FEBS Lett.* **585**, 104–110.
Golub, A. G., Bdzhola, V. G., Ostrynska, O. V., Kyshenia, I. V., Sapelkin, V. M., Prykhod'ko, A. O., Kukharenko, O. P. & Yarmoluk, S. M. (2013). *Bioorg. Med. Chem.* **21**, 6681–6689.
Hochschref, J., Schnitzler, A. & Issinger, O. (2015). *Protein Kinase CK2 Cellular Function in Normal and Disease State*, edited by K. Ahmed, O. Issinger & R. Szyszka, pp. 17–34. Cham: Springer.
Huse, M. & Kuriyan, J. (2002). *Cell*, **109**, 275–282.
Janeczko, M., Masłyk, M., Szyszka, R. & Baier, A. (2011). *Mol. Cell. Biochem.* **356**, 121–126.
Johnson, L. N., Noble, M. E. M. & Owen, D. J. (1996). *Cell*, **85**, 149–158.
Kabsch, W. (2010). *Acta Cryst.* D**66**, 125–132.
Kabsch, W. & Sander, C. (1983). *Biopolymers*, **22**, 2577–2637.
Kinoshita, T., Nakaniwa, T., Sekiguchi, Y., Sogabe, Y., Sakurai, A., Nakamura, S. & Nakanishi, I. (2013). *J. Synchrotron Rad.* **20**, 974–979.
Koltun, E. S., Tsuhako, A. L., Brown, D. S., Aay, N., Arcalas, A., Chan, V., Du, H., Engst, S., Ferguson, K., Franzini, M., Galan, A., Holst, C. R., Huang, P., Kane, B., Kim, M. H., Li, J., Markby, D., Mohan, M., Noson, K., Plonowski, A., Richards, S. J., Robertson, S., Shaw, K., Stott, G., Stout, T. J., Young, J., Yu, P., Zaharia, C. A., Zhang, W., Zhou, P., Nuss, J. M., Xu, W. & Kearney, P. C. (2012). *Bioorg. Med. Chem. Lett.* **22**, 3727–3731.
Kufareva, I., Bestgen, B., Brear, P., Prudent, R., Laudet, B., Moucadel, V., Ettaoussi, M., Sautel, C. F., Krimm, I., Engel, M., Filhol, O., Borgne, M. L., Lomberget, T., Cochet, C. & Abagyan, R. (2019). *Sci. Rep.* **9**, 15893.
Legrand, P. (2017). *xdsme: XDS Made Easier*. https://github.com/legrandp/xdsme.
Liebschner, D., Afonine, P. V., Baker, M. L., Bunkóczi, G., Chen, V. B., Croll, T. I., Hintze, B., Hung, L.-W., Jain, S., McCoy, A. J., Moriarty, N. W., Oeffner, R. D., Poon, B. K., Prisant, M. G., Read, R. J., Richardson, J. S., Richardson, D. C., Sammito, M. D., Sobolev, O. V., Stockwell, D. H., Terwilliger, T. C., Urzhumtsev, A. G., Videau, L. L., Williams, C. J. & Adams, P. D. (2019). *Acta Cryst.* D**75**, 861–877.
Liu, H., Wang, H., Teng, M. & Li, X. (2014). *Acta Cryst.* D**70**, 501–513.
Lozeman, F. J., Litchfield, D. W., Piening, C., Takio, K., Walsh, K. A. & Krebs, E. G. (1990). *Biochemistry*, **29**, 8436–8447.
Marta, R., Vélez-Bermudez, I. C., Legnaioli, T. & Montserrat, P. (2013). *Protein Kinase CK2*, edited by L. Pinna, pp. 267–279. Ames: Wiley-Blackwell.
McCoy, A. J., Grosse-Kunstleve, R. W., Adams, P. D., Winn, M. D., Storoni, L. C. & Read, R. J. (2007). *J. Appl. Cryst.* **40**, 658–674.
Meggio, F. & Pinna, L. A. (2003). *FASEB J.* **17**, 349–368.
Moreno-Romero, J., Armengot, L., Marquès-Bueno, M. M., Britt, A. & Martínez, M. C. (2012). *Plant J.* **71**, 627–638.
Mulekar, J. J. & Huq, E. (2014). *J. Exp. Bot.* **65**, 2883–2893.
Niefind, K., Bischoff, N., Golub, A. G., Bdzhola, V. G., Balanda, A. O., Prykhod'ko, A. O. & Yarmoluk, S. M. (2017). *Pharmaceuticals*, **10**, E9.
Niefind, K., Guerra, B., Ermakowa, I. & Issinger, O.-G. (2001). *EMBO J.* **20**, 5320–5331.
Niefind, K., Guerra, B., Pinna, L. A., Issinger, O.-G. & Schomburg, D. (1998). *EMBO J.* **17**, 2451–2462.
Niefind, K. & Issinger, O.-G. (2010). *Biochim. Biophys. Acta*, **1804**, 484–492.

Niefind, K., Pütter, M., Guerra, B., Issinger, O.-G. & Schomburg, D. (1999). *Nat. Struct. Biol.* **6**, 1100–1103.
Niefind, K., Raaf, J. & Issinger, O.-G. (2009). *Cell. Mol. Life Sci.* **66**, 1800–1816.
Ong, B. X., Yoo, Y., Han, M. G., Park, J. B., Choi, M. K., Choi, Y., Shin, J.-S., Bahn, Y.-S. & Cho, H.-S. (2019). *Sci. Rep.* **9**, 14398.
Pinna, L. A. (1997). *Int. J. Biochem. Cell Biol.* **29**, 551–554.
Pinna, L. A. & Meggio, F. (1997). *Prog. Cell Cycle Res.* **3**, 77–97.
Raaf, J., Brunstein, E., Issinger, O.-G. & Niefind, K. (2008). *Chem. Biol.* **15**, 111–117.
Raaf, J., Guerra, B., Neundorf, I., Bopp, B., Issinger, O.-G., Jose, J., Pietsch, M. & Niefind, K. (2013). *ACS Chem. Biol.* **8**, 901–907.
Ruiz-Carrillo, D., Lin, J., El Sahili, A., Wei, M., Sze, S. K., Cheung, P. C. F., Doerig, C. & Lescar, J. (2018). *Sci. Rep.* **8**, 7365.
Sajnaga, E., Szyszka, R. & Kubiński, K. (2013). *Genetic Manipulation of DNA and Protein. Examples from Current Research*, edited by D. Figurski, pp 133–166. London: IntechOpen.
Salinas, P., Fuentes, D., Vidal, E., Jordana, X., Echeverria, M. & Holuigue, L. (2006). *Plant Cell Physiol.* **47**, 1295–1308.
Sarno, S., Papinutto, E., Franchin, C., Bain, J., Elliott, M., Meggio, F., Kazimierczuk, Z., Orzeszko, A., Zanotti, G., Battistutta, R. & Pinna, L. A. (2011). *Curr. Top. Med. Chem.* **11**, 1340–1351.
Steichen, J. M., Kuchinskas, M., Keshwani, M. M., Yang, J., Adams, J. A. & Taylor, S. S. (2012). *J. Biol. Chem.* **287**, 14672–14680.
Tsuyuguchi, M., Nakaniwa, T., Hirasawa, A., Nakanishi, I. & Kinoshita, T. (2020). *Bioorg. Med. Chem. Lett.* **30**, 126837.
Velez-Bermudez, I. C., Irar, S., Carretero-Paulet, L., Pagès, M. & Riera, M. (2011). *Mol. Cell. Biochem.* **356**, 255–260.
Vilela, B., Pagès, M. & Riera, M. (2015). *Front. Plant Sci.* **6**, 966.